



## RESEARCH ARTICLE

# Structure or Exchange? On the Feasibility of Chemical Exchange Detection with Balanced Steady-State Free Precession in Tissue – An In Vitro Study

Rahel Heule<sup>1</sup>  | Anagha Deshmane<sup>1</sup>  | Moritz Zaiss<sup>1</sup>  | Kai Herz<sup>1</sup> | Philipp Ehses<sup>2</sup> | Klaus Scheffler<sup>1,3</sup>

<sup>1</sup> High Field Magnetic Resonance, Max Planck Institute for Biological Cybernetics, Tübingen, Germany

<sup>2</sup> German Center for Neurodegenerative Diseases (DZNE), Bonn, Germany

<sup>3</sup> Department of Biomedical Magnetic Resonance, University of Tübingen, Tübingen, Germany

## Correspondence

Rahel Heule, PhD, High Field Magnetic Resonance, Max Planck Institute for Biological Cybernetics, Max-Planck-Ring 11, 72076 Tübingen, Germany.  
Email: rahel.heule@tuebingen.mpg.de

## Funding information

German Research Foundation, Grant/Award Number: DFG, grant ZA 814/2-1 Reinhart Koselleck Project, DFG SCHE 658/12; European Union's Horizon 2020 research and innovation program, Grant/Award Number: 667510; Max Planck Society

Balanced steady-state free precession imaging has recently been suggested for chemical exchange detection (bSSFPX). The objective of this work is to investigate the contributions of microstructural, chemical shift and chemical exchange effects to the asymmetry of the bSSFP profile at field strengths of 3 T and 9.4 T. To this end, *in vitro* bSSFPX experiments are performed for a range of repetition times and flip angles in glucose water solutions with different  $\text{MnCl}_2$  concentrations and tissue homogenates obtained from the brainstem of pig brains. The experimental results are compared to multi-pool Bloch-McConnell simulations. Additionally, the influence of white matter tract geometry is analyzed *ex vivo* in pig brain hemispheres measured at two different angles with respect to  $B_0$ .

The detectable bSSFP profile asymmetry in glucose solutions with tissue-like relaxation times and white matter homogenates was consistent with Bloch-McConnell simulations but relatively small. In intact white matter tracts, the asymmetry was dominated by structural effects with a strong dependency on tract orientation relative to  $B_0$ . In tracts perpendicular to  $B_0$ , the asymmetry was  $\approx 3$ -4 times higher than in the homogenates, thus barely affected by chemical exchange effects. In conclusion, chemical exchange-related bSSFP profile asymmetries are detectable in tissue homogenates, however, the observed asymmetry level is generally low and prone to confounding structural effects rendering *in vivo* chemical exchange detection with bSSFP challenging in the brain.

## KEYWORDS

bSSFP, profile asymmetry, chemical exchange, glucose, white matter, pig brain

## 1 | INTRODUCTION

The MR signal acquired with a balanced steady-state free precession (bSSFP) sequence is known to be considerably off-resonance sensitive<sup>1</sup> and thus to carry information about the frequency content in a voxel. Tissues can generally not be described by a single  $T_1$ ,  $T_2$ , and resonance

**Abbreviations:** AI, asymmetry index; AREX, apparent exchange-dependent relaxation; APT, amide proton transfer;  $B_0/B_1$ , static/transmit magnetic field; bSSFP, balanced steady-state free precession; CEST, chemical exchange saturation transfer;  $\text{MnCl}_2$ , manganese (II) chloride monohydrate; MPRAGE, magnetization-prepared rapid gradient-echo; MT, magnetization transfer;  $\text{MTR}_{\text{Rex}}$ , spillover-corrected inverse magnetization transfer ratio; NOE, nuclear Overhauser enhancement; PBS, phosphate-buffered saline; RF, radiofrequency; ROI, region-of-interest; SAR, specific absorption rate; MT, semi-solid magnetization transfer; WASABI, water shift and  $B_1$

The copyright line for this article was changed on 19 October 2020 after original online publication.

This is an open access article under the terms of the Creative Commons Attribution-NonCommercial License, which permits use, distribution and reproduction in any medium, provided the original work is properly cited and is not used for commercial purposes.

© 2019 The Authors. NMR in Biomedicine published by John Wiley & Sons Ltd

frequency, but rather by multi-component relaxation and a distribution of frequencies. The voxel frequency distribution in tissues is highly likely to be asymmetric due to the presence of different frequency-shifted compartments. This in turn causes asymmetries in the bSSFP frequency profile, i.e. in the bSSFP signal assessed across a range of frequencies. The bSSFP frequency response is thus thought to be directly linked to tissue microstructure.

Asymmetries in the bSSFP frequency profile of tissues were first measured in 2010 using a series of phase-cycled acquisitions.<sup>2,3</sup> In these seminal studies, the authors observed bSSFP profile asymmetries in brain tissue and muscle. Pronounced asymmetries were seen especially in white matter structures<sup>2</sup> exhibiting a strong sensitivity to the orientation of the fiber tracts with the largest asymmetries occurring in tracts perpendicular to the static magnetic field ( $B_0$ ).<sup>3,4</sup> These results suggest a relation to anisotropies in the tissue microenvironment, possibly driven by susceptibility-shifted molecules due to fiber tract geometry.<sup>5,6</sup>

On the other hand, bSSFP imaging was only recently reported to be intrinsically sensitive to chemical exchange processes leading to asymmetric profiles in isotropic probes of exchanging molecular species.<sup>7</sup> The authors demonstrated based on *in vitro* experiments that phase-cycled bSSFP, in this context termed bSSFPX, is able to detect chemical exchange processes in solute molecules with small chemical shift differences of the dominant pool close to 1 ppm, such as choline, glucose and glycogen water solutions. The provided contrast in the measured probes related to chemical exchange was observed to be comparable with standard chemical exchange saturation transfer (CEST) measurements.<sup>7</sup> Based on these results, the authors hypothesized that the bSSFP sequence may perform well for studies investigating glucose infusion into brain tumors similar to glucoCEST.<sup>8</sup>

The observed sensitivity of the bSSFP frequency response to chemical exchange raises a number of questions. It remains unclear whether it may be feasible to assess chemical exchange effects in healthy or possibly tumorous tissues with bSSFPX. To date, the only reported experiments were performed in water solutions characterized by long  $T_1$  and  $T_2$  relaxation times unlike tissue.<sup>7</sup> It also appears interesting to investigate whether exchanging chemical moieties contribute to the pronounced bSSFP profile asymmetries observed in white matter or whether they are caused by purely structural effects related to the geometry of the fiber tracts. At low RF power as inherent to bSSFP imaging due to gradient hardware and SAR limitations, the chemical exchange processes in human brain tissues are governed by the nuclear Overhauser enhancement (NOE) effects occurring upfield from water at -3.5 ppm.<sup>9,10</sup> Standard CEST imaging at ultra-high fields has not only demonstrated an easier separation of the peaks but also an increase in the effect strength for amide, amine, and NOE pools.<sup>11</sup> bSSFPX, on the other hand, is expected to show a complex behavior with increasing field strength due to the periodicity of the bSSFP frequency response with  $1/TR$ , which results in CEST-related asymmetries at pool offsets larger than  $1/TR$  folding back into the profile and consequently an overlap of CEST pools at different chemical shifts.<sup>7</sup>

In this work, the above questions are explored by means of *in vitro* glucose and pig brain tissue experiments at field strengths of 3 T and 9.4 T. Phase-cycled bSSFP profile measurements are established for chemical exchange detection in glucose water solutions, examining the dependencies on relaxation time, flip angle ( $\alpha$ ), repetition time (TR), and field strength ( $B_0$ ). The results are compared to multi-pool Bloch-McConnell simulations. Similar experiments and simulations are performed based on probes containing homogenized fresh pig brain tissue from the brainstem to eliminate structural effects as possible source for the observed asymmetries. In addition, intact pig brain hemispheres are measured *ex vivo* at different angles with respect to  $B_0$  providing reference asymmetry indices (AI) in white matter structures. At 9.4 T, the pig brain tissue measurements are accompanied by a standard CEST acquisition<sup>9,12</sup> to validate the pools which govern the exchange processes and to compare the effect strength in the homogenate with intact white matter tissue.

## 2 | EXPERIMENTAL

The postprocessing of the acquired MR data and the visualization of the results were done using Matlab R2017a (The MathWorks, Inc., Natick, MA). The MR scans were performed at 3 T (Magnetom Prisma, Siemens Healthcare, Erlangen, Germany) using the standard 64-channel receive head coil of the manufacturer and at 9.4 T using a custom-built head coil array consisting of 18 transceiver surface loops and 14 receive-only vertical loops.<sup>13</sup>

### 2.1 | Phantom preparation

D-glucose solutions were prepared in three 20 ml tubes at a concentration of 100 mM diluted in distilled water and containing different concentrations of manganese (II) chloride monohydrate ( $MnCl_2$ ) to adjust the relaxation times: 0 mM (probe 1), 0.03 mM (probe 2), and 0.06 mM (probe 3). The obtained solutions were characterized by a pH of 5.9 and nominal  $T_1/T_2$  values of 3620 ms / 408 ms (probe 1), 1940 ms / 149 ms (probe 2), 1300 ms / 91 ms (probe 3) at 3 T as well as 3960 ms / 363 ms (probe 1), 2120 ms / 110 ms (probe 2), 1460 ms / 65 ms (probe 3) at 9.4 T, assessed using gold standard inversion-recovery spin echo scans for  $T_1$  and single-echo spin echo scans for  $T_2$  measurements.

The three probes were placed in the center of a cylindrical phantom container which was filled with phosphate-buffered saline (PBS) doped by 0.05 mM  $\text{MnCl}_2$ .

White matter tissue samples were collected from the brainstem of fresh pig brains and homogenized in a two-step process. First, a blender, i.e. a blade homogenizer, was used for premixing. Then, the final homogenate was obtained by sonication on ice for 4 min. During the homogenization process, tiny air bubbles formed in the homogenate. For this reason, the homogenate was diluted by PBS and centrifuged to force the air to surface. To investigate the effect of dilution, three 20 ml probes were prepared with different tissue to PBS ratios. One of them was only marginally diluted to approximate *in vivo* conditions:  $V_{\text{tissue}}/(V_{\text{tissue}}+V_{\text{PBS}}) = 17/20$  (homogenate 1), 2/3 (homogenate 2), and 1/2 (homogenate 3), where  $V_{\text{tissue}}$  is the tissue volume and  $V_{\text{PBS}}$  the volume of PBS. According to gold standard reference scans, the obtained homogenates were characterized by nominal  $T_1/T_2$  values of 1240 ms / 94 ms (homogenate 1), 1570 ms / 133 ms (homogenate 2), 1690 ms / 164 ms (homogenate 3) at 3 T as well as 1920 ms / 43 ms (homogenate 1), 2110 ms / 64 ms (homogenate 2), 2260 ms / 77 ms (homogenate 3) at 9.4 T. Similar to the glucose phantom, the three probes were placed in the middle of a cylindrical container (container contents: PBS / 0.05 mM  $\text{MnCl}_2$ ). The 3 T and 9.4 T measurements were performed on the same day using the same homogenates.

To obtain reference asymmetry indices in intact tissue, a phantom holding a fresh pig brain hemisphere was prepared. The brain hemisphere was first immersed in PBS and subjected to vacuum pumping to eliminate air bubbles along with filling the air cavities by liquid. Then it was transferred to a cylindrical phantom holder and embedded in 2% agar. The scanned pig brain hemispheres were not identical for the two investigated field strengths as the measurements were performed on different days.

## 2.2 | MR acquisition protocol

The response of the bSSFP signal to a frequency offset  $\Delta f$  is equivalent to an RF phase cycling with linear increment  $\varphi = 2\pi\Delta f \cdot TR$ . Consequently, to sample the bSSFP frequency profile, a series of 60 phase-cycled 3D bSSFP scans was performed with RF phase increments  $\varphi$  covering a range of  $400^\circ$  in steps of  $6.66^\circ$  to acquire the entire bandwidth even in the presence of frequency drifts. Each phase-cycle was preceded by a dummy preparation module to ensure steady-state conditions. The bSSFP frequency response was investigated for a range of TRs and flip angles. The achievable flip angle was restricted by the specific absorption rate (SAR), which was relaxed in case of the glucose scans by switching the patient protection mode off. For each set of parameters [TR,  $\alpha$ ], the profile measurement was repeated with negative frequency sweep.

bSSFP TR and flip angle settings for the glucose phantom:

- At 3 T:
  - TR = 2.5 ms,  $\alpha_{\text{nom}} = [6, 8, 10, 12, 14, 16, 18, 20]^\circ$
  - TR = 4 ms,  $\alpha_{\text{nom}} = [6, 10, 14, 18, 22, 26, 30]^\circ$
  - $\alpha_{\text{nom}} = 20^\circ$ , TR = [2.5, 3.0, 3.5, 4.0, 4.5, 5.0, 5.5, 6.0] ms
- At 9.4 T:
  - TR = 2.5 ms,  $\alpha_{\text{nom}} = [6, 7, 8, 9, 10, 11, 12, 13, 14]^\circ$
  - TR = 4 ms,  $\alpha_{\text{nom}} = [6, 7, 8, 9, 10, 11, 12, 13, 14]^\circ$
  - $\alpha_{\text{nom}} = 11^\circ$ , TR = [2.5, 3.0, 3.5, 4.0, 4.5, 5.0, 5.5, 6.0] ms

bSSFP TR and flip angle settings for the homogenized pig brain tissue phantom:

- At 3 T:
  - TR = 2.5 ms,  $\alpha_{\text{nom}} = [12, 16, 20]^\circ$
  - TR = 4 ms,  $\alpha_{\text{nom}} = [10, 12, 14, 16, 18, 20, 25, 30]^\circ$
- At 9.4 T:
  - TR = 2.5 ms,  $\alpha_{\text{nom}} = [6, 7]^\circ$
  - TR = 4 ms,  $\alpha_{\text{nom}} = [6, 7, 8, 9, 10, 11]^\circ$

The bSSFP profile measurements of the intact pig brain hemisphere were performed for TR = 4 ms /  $\alpha_{\text{nom}} = 12^\circ$  at 3 T and TR = 4 ms /  $\alpha_{\text{nom}} = 11^\circ$  at 9.4 T.

Overall, the TR and flip angle range investigated in the glucose and homogenized/intact pig brain tissue phantoms translates to a nominal mean  $B_1$

field in the range of [0.10, 0.52]  $\mu\text{T}$  using the formula  $B_{1,\text{mean}} = \int_0^{TR} B_1(t) dt / TR = \alpha / (360\gamma TR)$ .<sup>7</sup>

bSSFP geometry parameters:

- Glucose: resolution =  $2 \times 2 \times 3 \text{ mm}^3$ , image matrix size =  $80 \times 80 \times 26$
- Homogenized pig brain tissue: resolution =  $2 \times 2 \times 2.25 \text{ mm}^3$  for TR = 2.5 ms /  $1.67 \times 1.67 \times 2.25 \text{ mm}^3$  for TR = 4 ms, image matrix size =  $80 \times 80 \times 36$  for TR = 2.5 ms /  $96 \times 96 \times 36$  for TR = 4 ms
- Pig brain hemisphere: resolution =  $1.46 \times 1.46 \times 2 \text{ mm}^3$ , image matrix size =  $96 \times 84 \times 20$
- 100% oversampling in partition encoding direction for all scans

Depending on TR and resolution, the total scan time for one bSSFP profile measurement ranged between 13 to 29 min. The bSSFP experiments were accompanied by a transmit field mapping sequence to estimate the transmit magnetic field ( $B_1$ ) scaling factor  $c_{B1} = \alpha_{\text{act}} / \alpha_{\text{nom}}$  ( $\equiv$  actual/nominal flip angle) voxelwise based on two 2D multi-slice gradient-echo acquisitions with and without a preconditioning RF pulse (TR = 8000 ms,  $\alpha_{\text{nom}} = 8^\circ$ ).<sup>14,15</sup>

At 9.4 T, the measurements of the pig brain phantom (homogenized and intact) included a standard CEST acquisition for reference. CEST imaging was performed using spectrally but not spatially selective saturation consisting of a train of Gaussian-shaped RF pulses with a total saturation period of 4.5 s (150 pulses of duration 15 ms and 50% duty cycle) and nominal  $B_1$  values of  $B_{1,\text{mean}} = [0.6, 0.9, 1.2] \mu\text{T}$ .<sup>9</sup> The presaturation module was followed by image acquisition with a centric-spiral reordered 3D gradient-echo readout (TR = 3.8 ms / 3.9 ms for the homogenized/intact pig brain phantom,  $\alpha_{\text{nom}} = 5^\circ$ ).<sup>12</sup> The Z-spectra were sampled at 95 offsets ranging from -50 to 50 ppm and an additional reference image was acquired at -300 ppm. For field inhomogeneity correction of the acquired Z-spectra,  $B_0$  and  $B_1$  field maps were simultaneously estimated based on the WASABI (water shift and  $B_1$ ) method.<sup>16</sup> Adiabatic saturation recovery scans were used to obtain  $T_1$ -compensated AREX (apparent exchange-dependent relaxation) CEST spectra.<sup>17,18</sup>

The experiments in the intact pig brain hemispheres were complemented by an anatomical scan using a conventional magnetization-prepared rapid gradient-echo (MPRAGE) contrast<sup>19</sup> with TR = 2000 ms / 4000 ms, inversion time TI = 1200 ms / 1500 ms, and  $\alpha_{\text{nom}} = 8^\circ / 9^\circ$  at 3 T / 9.4 T. Additionally, a standard diffusion-tensor imaging experiment was performed at 3 T using a 2D spin-echo echo-planar imaging sequence in multi-directional diffusion weighting mode along 30 diffusion directions at two different b-values ( $2000 \text{ s/mm}^2$  and  $4000 \text{ s/mm}^2$ ). A single non-diffusion weighted dataset with  $b = 0 \text{ s/mm}^2$  was also acquired. The derived color-coded fiber direction map provided a reference to select regions-of-interest (ROIs) in white matter structures with high fractional anisotropy and known fiber tract orientation with respect to  $B_0$ .

## 2.3 | BSSFP and CEST data analysis

Gibbs ringing artifacts in the acquired 3D bSSFP datasets were removed using local subvoxel shifts.<sup>20</sup> At 9.4 T, the observed phase drift during the duration of the bSSFP profile measurements was only minor. Therefore, phase-cycles that overlapped within a modulo range of  $360^\circ$  were averaged, resulting in 54 phase-cycles. At 3 T, 60 phase-cycles described the entire bandwidth better due to a more pronounced drift and were thus all retained. Then, the bSSFP profiles were voxelwise centered, i.e.  $B_0$ -corrected, based on the profile pattern and its second derivative.<sup>2</sup> In a second step, residual subsample frequency shifts were corrected by fitting the profile to a smoothing spline, determining the center frequency as the maximum of the second derivative of the fit, and then interpolating the non-fitted profiles according to this center frequency.<sup>3</sup> The final profile was calculated as the average of the centered profiles acquired with positive and negative frequency sweeps to exclude transient effects that were seen to cause profile asymmetries.<sup>2</sup>

The degree of bSSFP profile asymmetry was assessed voxelwise by the normalized asymmetry index (AI) defined as

$$AI = \frac{A_n - A_p}{A_n + A_p} \quad (1)$$

where  $A_{n,p}$  is the area under the profile at negative (n) and positive (p) frequency offsets relative to the banding. At 9.4 T where the  $B_1$  field is highly inhomogeneous, the profiles and corresponding asymmetry indices derived from scans with varying flip angles but otherwise identical parameters were binned for selected ROIs according to their actual flip angle  $\alpha_{\text{act}} = c_{B1} \cdot \alpha_{\text{nom}}$  and subsequently averaged.

The Z-spectrum data acquired with standard CEST experiments were first  $B_0$ - and  $B_1$ -corrected using the WASABI approach<sup>16</sup> in combination with a three-point Z- $B_1$ -correction method based on the three acquisitions at nominal  $B_{1,\text{mean}} = [0.6, 0.9, 1.2] \mu\text{T}$ <sup>18</sup> and subsequently reconstructed at an actual irradiation amplitude of  $B_{1,\text{mean}} = 0.5 \mu\text{T}$ . This power has been reported to provide high selectivity as well as strong CEST effects<sup>9</sup> and matches the maximal RF power of the bSSFP acquisitions. The nominal  $B_{1,\text{mean}}$  values were set up higher than the actual reconstructed one since the voxelwise  $B_1$  scaling factor  $c_{B1}$  in the regions-of-interest used to calculate mean Z-spectra was rather low, i.e. in the range [0.4, 0.9]. The final Z-spectra  $Z(\Delta\omega)$  were derived as the ratio of the saturated image and the fully relaxed reference image obtained at  $\Delta\omega = -300 \text{ ppm}$ . The CEST effects were isolated from direct water saturation (spillover) and semi-solid magnetization transfer (MT) using 2-pool

Lorentzian fitting to estimate the background signal  $Z_{\text{fit,water,MT}}(\Delta\omega)$ .<sup>9</sup> To remove spillover dilution effects from the isolated CEST effects, the inverse magnetization transfer ratio metric,  $\text{MTR}_{\text{Rex}}(\Delta\omega)$ ,<sup>21</sup> was employed:

$$\text{MTR}_{\text{Rex}}(\Delta\omega) = \frac{1}{Z(\Delta\omega)} - \frac{1}{Z_{\text{fit,water,MT}}(\Delta\omega)} \quad (2)$$

An additional correction for the  $T_1$  relaxation of the water pool was performed yielding the apparent exchange-dependent relaxation,  $\text{AREX}(\Delta\omega)$ <sup>17</sup>:

$$\text{AREX}(\Delta\omega) = \frac{1}{T_1} \text{MTR}_{\text{Rex}}(\Delta\omega) \quad (3)$$

## 2.4 | Multi-pool Bloch-McConnell simulations

Chemical exchange processes between solutes and free water protons were described using the Bloch-McConnell equations.<sup>22,23</sup> RF excitation pulses were modeled with a truncated SINC envelope as used in the experiments for slice selection. As specified by the manufacturer, nominal  $B_0$  values of 2.89 T ( $\equiv$  3 T) and 9.39 T ( $\equiv$  9.4 T) were used for the simulations.

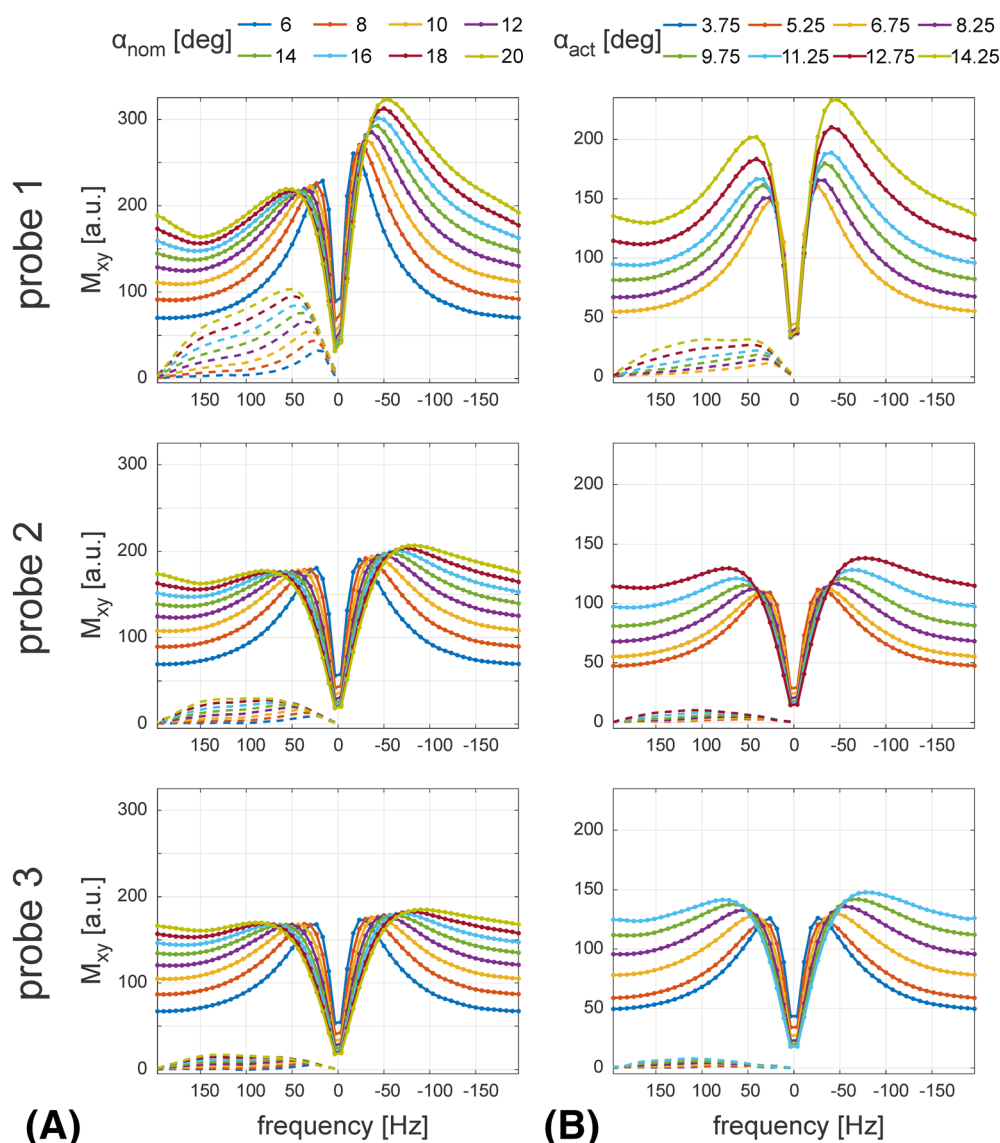


**FIGURE 1** Average bSSFP frequency profiles (solid curves) and corresponding non-normalized asymmetries (dashed curves) measured at 3 T (A) and 9.4 T (B), for a TR of 2.5 ms and varying flip angles in glucose water solutions with different  $\text{MnCl}_2$  concentrations: 0 mM (probe 1, first row), 0.03 mM (probe 2, second row), and 0.06 mM (probe 3, third row). At 9.4 T B the profiles were binned voxelwise according to their actual flip angle ( $\alpha_{\text{act}}$ ) obtained from a  $B_1$  mapping scan using a bin size of  $1.5^\circ$  and then averaged

The prepared glucose solutions were approximated by a 2-pool model, i.e. one bulk water pool referred to as "w" and one solute CEST pool referred to as "s". CEST effects were assumed to be governed by exchanging hydroxyl groups resonating at  $\Delta_s = 1.28$  ppm downfield from water with a relative pool size of  $f_s = 0.0027$  ( $\equiv$  three effective protons at a concentration of 100 mM<sup>8</sup>), exchange rate  $k_s = 550$  Hz (for pH = 5.9 at 21° C<sup>24</sup>), and  $T_{1s} = T_{2s} = 1$  s. If not otherwise stated, the relaxation times  $T_{1w}$  and  $T_{2w}$  of the water pool were set to the measured values in the glucose probe 1 and the MR protocol parameters  $TR = 2.5$  ms /  $\alpha_{nom} = 14^\circ$  were used.

To simulate the white matter tissue response to bSSFPX, a 3-pool model was used including one water pool ("w"), one CEST pool ("s"), and one magnetization transfer (MT) pool ("m"). Semi-solid macromolecular MT effects were described based on the Bloch-McConnell model by neglecting the transverse components due to the rapid transverse relaxation of the MT pool<sup>25</sup> and assuming a Lorentzian lineshape, thus treating MT like a broad CEST effect.<sup>26</sup> Possible exchange processes between the MT and CEST pool were considered negligible. CEST effects were assumed to arise predominantly from the NOE at the used low power. If not otherwise stated, a TR of 4 ms,  $\alpha_{nom} = 10^\circ$ , and the following pool parameters were used:  $\Delta_s = -3.6$  ppm /  $f_s = 0.01$  /  $k_s = 27$  Hz /  $T_{1s} = T_{1w}$  /  $T_{2s} = 5$  ms (CEST pool, NOE<sup>27,28</sup>),  $\Delta_m = -2.5$  ppm /  $f_m = 0.1$  /  $k_m = 23$  Hz /  $T_{1m} = T_{1w}$  /  $T_{2m} = 10$   $\mu$ s (MT pool<sup>29,30</sup>), and  $T_{1w}/T_{2w}$  (water pool) set to the measured values in the homogenate obtained with minimal dilution (homogenate 1).

### 3 | RESULTS

Representative bSSFP profiles measured in glucose solutions are displayed in Figure 1 obtained at 3 T (Fig. 1a) and 9.4 T (Fig. 1b) for a TR of 2.5 ms at different flip angles. Pronounced asymmetries can be seen, in particular in probe 1 at 3 T, which are increasing with higher flip angles. It is evident that the observable asymmetry in probes 2 and 3 with rather tissue-like relaxation times is reduced to a high degree as compared to probe 1. The bSSFP profile asymmetry is quantified in Figure 2 by the asymmetry index AI (c.f. Eq. [1]), demonstrating a clear dependence on TR and flip angle with higher measured AIs at shorter TRs and increasing flip angles for both field strengths but generally weaker asymmetry at 9.4 T in comparison to 3 T for the investigated parameter range. Shorter relaxation times in the tissue regime corresponding to higher MnCl<sub>2</sub> concentrations lead to considerably reduced AI values (cf. probes 2 and 3 to probe 1 in Fig. 2).

The results obtained for glucose bSSFPX are corroborated by 2-pool Bloch-McConnell simulations shown in Figure 3 which yield similar dependencies on relaxation times and protocol parameters (TR,  $\alpha$ ) as in the measurements. The bSSFP profile asymmetry decreases considerably when approaching tissue-like  $T_1$  and  $T_2$  as illustrated for TR = 2.5 ms and  $\alpha = 14^\circ$  (cf. Figs. 3a+b) with generally higher AI values at 3 T (Fig. 3a)

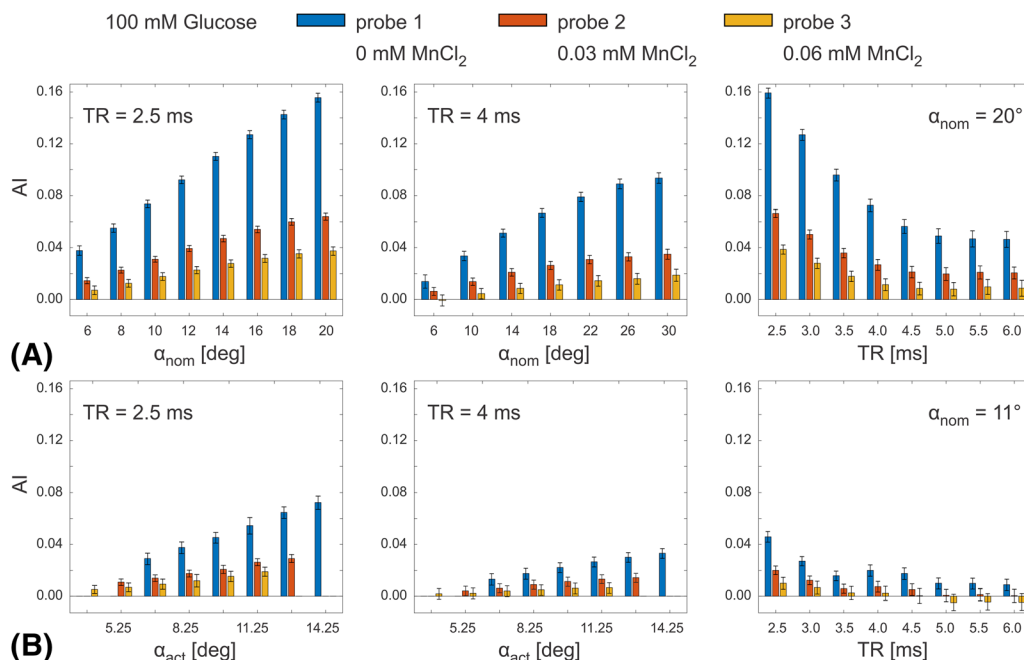


**FIGURE 2** Quantitative assessment of chemical exchange effects in glucose solutions at 3 T (A) and 9.4 T (B) using the asymmetry index (AI) defined in Eq. [1]. The results for different TR and flip angle settings are displayed. For the scans at 9.4 T with fixed TR and varying flip angles (B left and middle), the asymmetry indices were binned voxelwise according to the corresponding B<sub>1</sub>-corrected actual flip angle ( $\alpha_{act}$ ) using a bin size of 1.5° and then averaged. The error bars indicate the standard deviation of the mean in the assessed ROIs



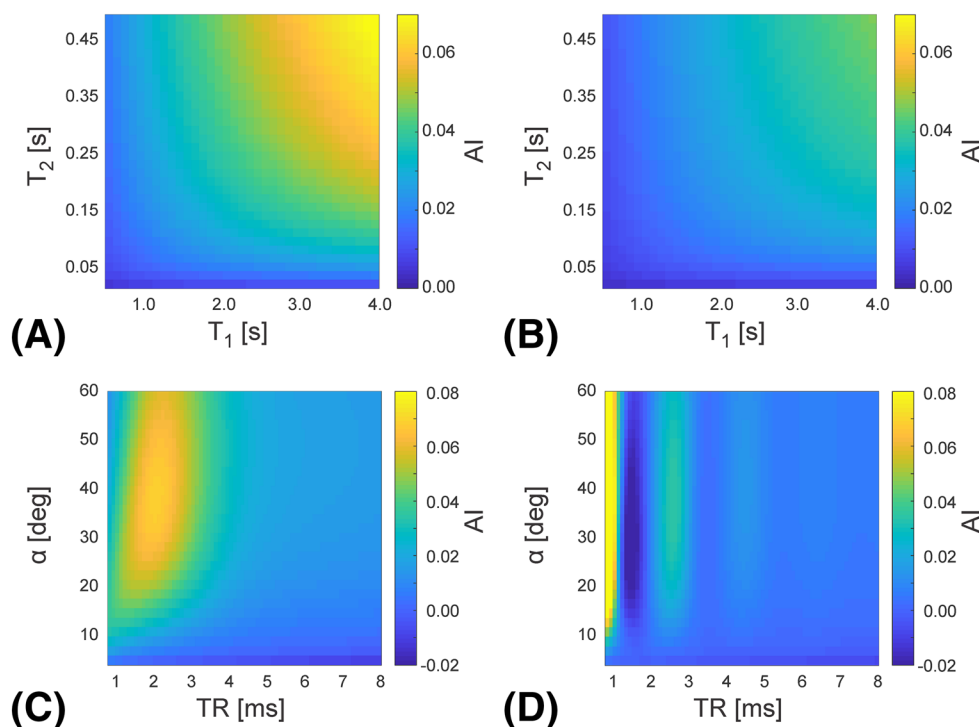


**FIGURE 3** Two-pool Bloch-McConnell simulations describing chemical exchange effects in glucose water solutions at 3 T (A, C) and at 9.4 T (B, D). A, B, Simulations are performed for a TR of 2.5 ms and a flip angle of  $14^\circ$  versus longitudinal and transverse relaxation times. C, D Simulations are performed versus repetition time and flip angle for  $T_1$  and  $T_2$  measured in probe 2 (100 mM glucose, 0.03 mM  $\text{MnCl}_2$ )

compared to 9.4 T (Fig. 3b) in agreement with the experiments. The simulations versus TR and flip angle yield AI values of the same order but somewhat lower as measured experimentally, e.g. 4.6% / 1.9% for TR = 2.5 ms at 3 T ( $\alpha = 20^\circ$ ) / 9.4 T ( $\alpha = 12.75^\circ$ ) versus 6.4% / 2.9% in the experiments (cf. Figs. 3c+d simulated for  $T_{1w}/T_{2w}$  of probe 2 versus Figs. 2a+b, left column, red bars). It can be seen that there exist optimal TR and flip angle settings maximizing the asymmetry index (Fig. 3c+d). At larger TRs, the asymmetric behavior generally tends to disappear. At 9.4 T, the cyclic nature of bSSFPX in combination with the increased chemical shift of the CEST pool leads to a stronger TR dependence and the occurrence of negative asymmetry indices for the simulated TR range (Fig. 3d). Very short TRs of about  $\approx 1$  ms appear to be beneficial to assess glucose exchange with bSSFPX at 9.4 T.

BSSFP frequency profiles measured in tissue homogenates with different dilution factors at 3 T and 9.4 T are shown in Figure 4. At 3 T, a small but consistent residual asymmetry can be observed (Fig. 4a) which appears enhanced at 9.4 T (Fig. 4b). The quantitative asymmetry analysis according to Eq. [1] indicates that dilution only marginally affects the overall observable asymmetry (cf. Fig. 5). For both investigated field strengths, the bSSFP profile asymmetry exhibits a dependence on TR. In addition, at 9.4 T, the measured AI values increase considerably for higher flip angles. Due to SAR constraints, a lower flip angle regime was assessed at 9.4 T as opposed to 3 T.

The results of Bloch-McConnell simulations modeling white matter tissue as a 3-pool system (bulk water, MT, NOE) are illustrated in Figure 6. In Figures 6a+b, the dependency of the bSSFPX response on the exchange rate and offset of the CEST pool is explored. For NOE pool characteristics reported in literature ( $\Delta_s = -3.5$  ppm /  $k_s = 27$  Hz<sup>27</sup>), the periodic bSSFPX response is close to a maximum at both 3 T (Fig. 6a) and 9.4 T (Fig. 6b). The peak AI values at  $\Delta_s \approx -3.6$  ppm ( $\approx 1\%$  at 3 T,  $\approx 1.3\%$  at 9.4 T) are comparable to the experimentally measured ones with enhanced asymmetry at 9.4 T compared to 3 T (cf. Fig. 5, TR = 4 ms,  $\alpha = 10^\circ$ ). The bSSFPX response in white matter is strongly dependent on TR (cf. Figs. 6c+d) due to the large chemical shift of the NOE pool (here  $\Delta_s = -3.6$  ppm), in particular at ultra-high-field strength (Fig. 6d), with a cycle of  $1/(\gamma^- \Delta_s B_0)$ . The AI values vary with the flip angle, especially in the low flip angle regime ( $< 10^\circ$ ) as also observed in the measurements at 9.4 T (cf. Fig. 5).

In Figures 7 and 8, the influence of white matter tract orientation relative to  $B_0$  on the bSSFP profile asymmetry is investigated. Representative anatomical MPRAGE contrasts, color-coded fiber direction maps, and bSSFP AI maps obtained at 3 T are shown in Figure 7 for two different angles with respect to  $B_0$ ; initial (referred to as  $0^\circ$ ) and  $\approx 90^\circ$  rotated around the anterior-posterior axis). As can be seen from Figure 7, the AI values are strongly correlated with the fiber orientation of white matter tracts exhibiting minimal asymmetry for white matter structures parallel to  $B_0$  (blue color-coding) and maximal asymmetry for tracts oriented perpendicular relative to  $B_0$  (green and red

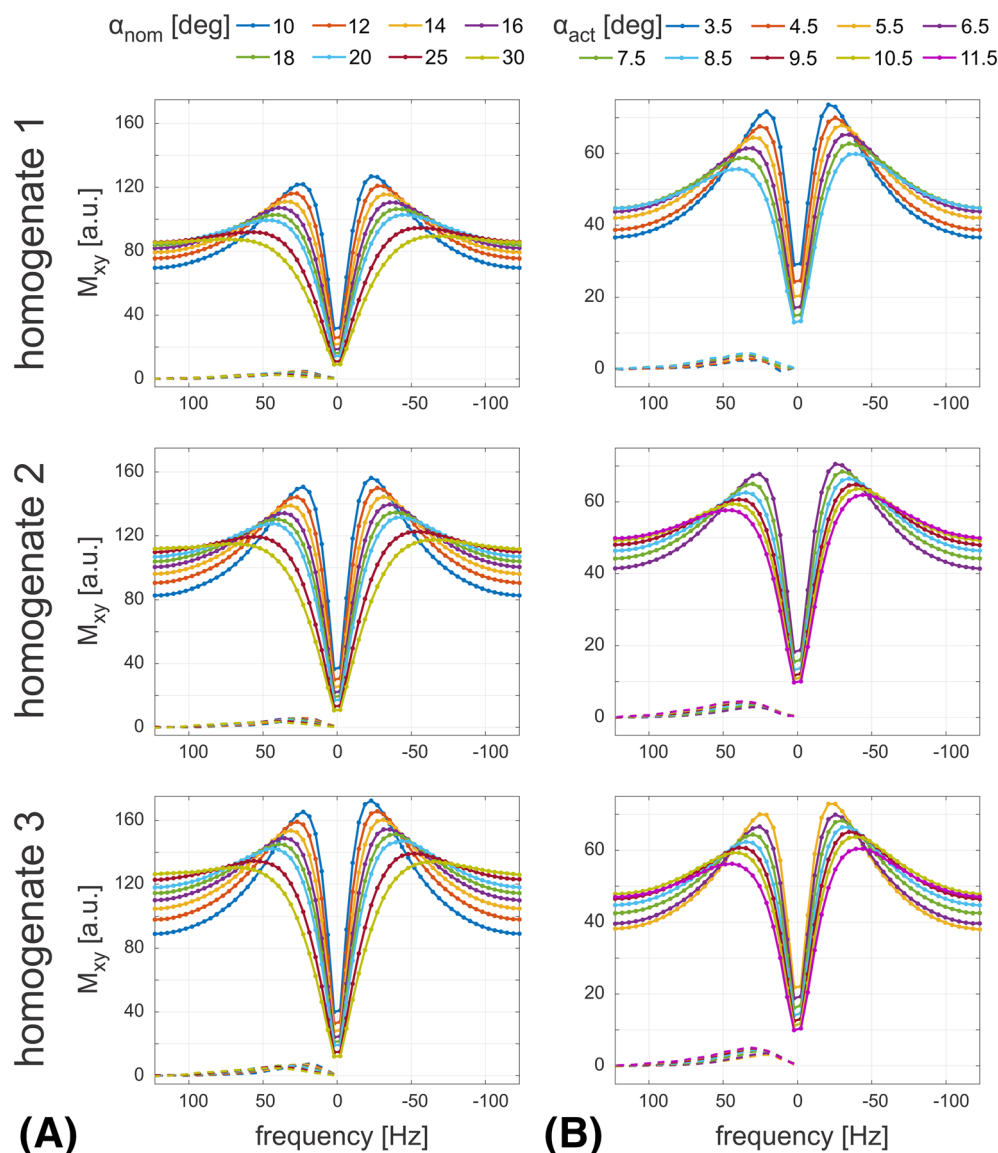


**FIGURE 4** bSSFP frequency profile measurements (solid curves) and corresponding non-normalized asymmetries (dashed curves) in homogenized white matter tissue samples of pig brains obtained with a TR of 4 ms and a range of flip angles at 3 T (A) and 9.4 T (B). The measured homogenates were diluted by PBS during the preparation process yielding the following tissue volume fractions (cf. 'Methods' section): 17/20 (homogenate 1, first row), 2/3 (homogenate 2, second row), 1/2 (homogenate 3, third row). At 9.4 T B a flip angle bin size of  $1^\circ$  was used for voxelwise binning and averaging of the measured profiles according to the  $B_1$ -corrected  $\alpha_{act}$

color-coding). These observations are manifest in Figure 8 where the bSSFP frequency profile is plotted in selected white matter ROIs for the initial positioning (blue curves) and  $\approx 90^\circ$  rotation (red curves). In white matter tracts which are aligned perpendicular to  $B_0$  ( $\theta_{B_0} \geq 70^\circ$ ), maximal AI values up to  $\approx 0.035$  can be observed at 3 T (Figs. 8a-c) whereas at 9.4 T higher AI values of up to  $\approx 0.06$  are found (Fig. 8d). In white matter tracts parallel to  $B_0$  ( $\theta_{B_0} \leq 20^\circ$ ), the asymmetry disappears to a large degree with a tendency to become slightly negative in the corticospinal tract (Figs. 8c+d). The AI values obtained in white matter tracts perpendicular to  $B_0$  are  $\approx 3$ -4 times higher as compared to the results in the homogenates.

On the other hand, as expected, standard CEST imaging does not show any dependence on fiber tract orientation relative to  $B_0$  as apparent from the Z-spectra assessed in the corticospinal tract at 9.4 T (Fig. 9a). The relaxation-compensated AREX contrast demonstrates that the chemical exchange processes in the homogenate are dominated by the NOE pool upfield from water at -3.5 ppm with a smaller effect downfield at +3.5 ppm caused by amide proton transfer (APT), cf. Fig. 9b, similar as reported in literature for *in vivo* white matter structures in the human brain.<sup>9,10</sup> The CEST effects in the homogenate with marginal dilution (homogenate 1) and in the corticospinal tract of intact pig brain hemispheres correspond well to each other.



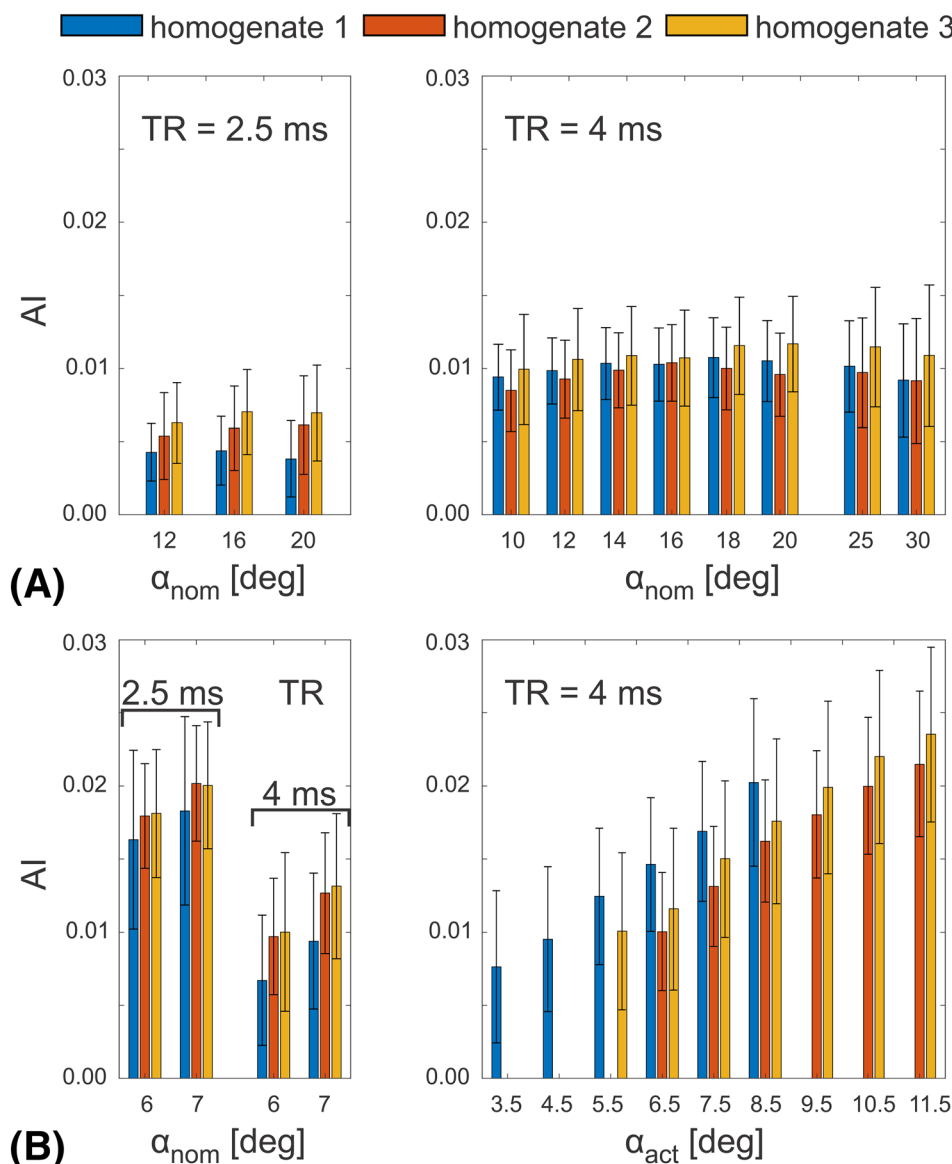


**FIGURE 5** Asymmetry indices (AI) obtained from bSSFPX experiments using two different TRs and varying flip angles at 3 T (A) and 9.4 T (B) in probes containing homogenized pig brain tissue with different tissue volume fractions (cf. 'Methods' section): 17/20 (homogenate 1), 2/3 (homogenate 2), 1/2 (homogenate 3). At 9.4 T, the AI values calculated for TR = 4 ms and a range of flip angles were binned according to their actual flip angle (B, right column). All other measurements were analyzed without flip angle binning. For direct comparison with the short TR measurement at 9.4 T, the AI values for the scans with TR = 4 ms at flip angles of 6° and 7° were recalculated without flip angle binning (B, left column). The error bars indicate the standard deviation of the mean in the assessed ROIs

## 4 | DISCUSSION

A theoretical framework describing the possibility of using the bSSFP frequency response for chemical exchange detection has been provided recently by Zhang et al.<sup>7</sup> In the respective work, the authors performed a few preliminary *in vitro* experiments to study molecules with small chemical shift differences in water solutions having long  $T_{1w}$  and  $T_{2w}$  values unlike tissue. Here, we investigated the potential of bSSFPX to be applied to *in vivo* settings by means of *in vitro* measurements in glucose serving as a simple single-solute model system in the slow-exchanging regime, white matter tissue homogenates, and *ex vivo* in intact fresh pig brain hemispheres.

As can be seen from the results obtained in glucose water solutions with varying  $\text{MnCl}_2$  concentrations, the observable asymmetry is strongly affected by both transverse and longitudinal relaxation times of the bulk water pool and tends to disappear for tissue-like values. A clear dependence on flip angle, TR, and  $B_0$  was observed in the experiments in agreement with Bloch-McConnell simulations. As evident from these simulations (cf. Fig. 3), very short TRs are required to maximize the profile asymmetries.

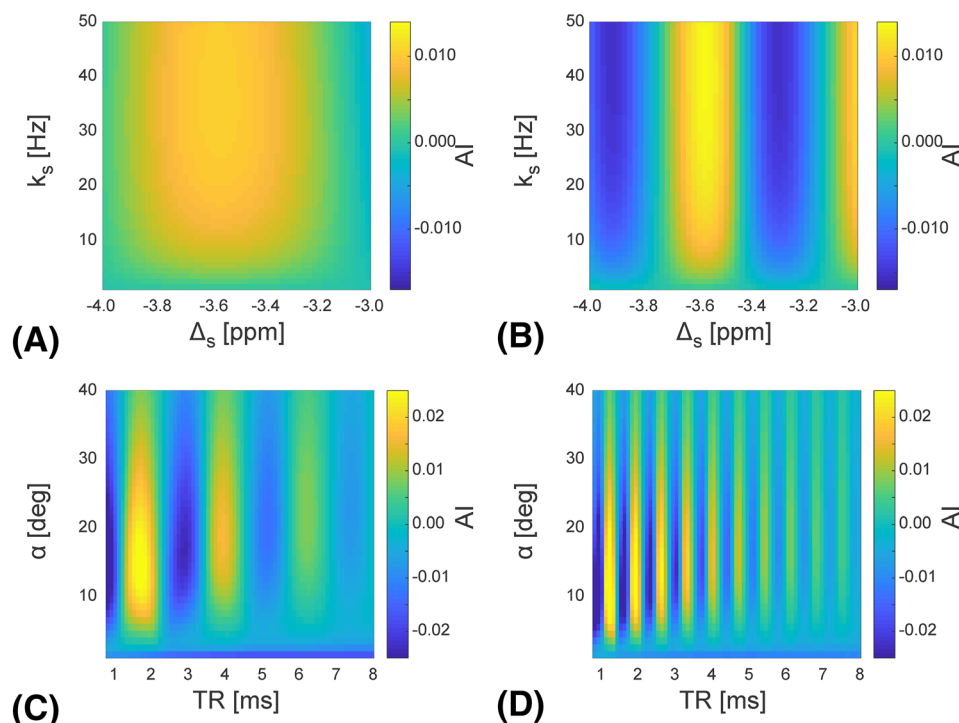


**FIGURE 6** The bSSFPX response in white matter is modeled by three-pool (bulk water, NOE, MT) Bloch-McConnell simulations for field strengths of 3 T (A, C) and 9.4 T (B, D). The  $T_1$  and  $T_2$  values were set to the relaxation times measured in the marginally diluted homogenate (homogenate 1). **A, B** Simulations are performed for a TR of 4 ms and a flip angle of  $10^\circ$  versus frequency offsets  $\Delta_s$  and exchange rates  $k_s$  of the CEST pool. As CEST effects in white matter are expected to be dominated by the NOE for the rather low RF power used, low exchange rates and frequency offsets close to -3.5 ppm are investigated which are assumed to characterize well the NOE pool. **C, D** Simulations are performed for  $\Delta_s = -3.6$  ppm and  $k_s = 27$  Hz versus repetition time and flip angle

In this work, the glucose solutions were characterized by a pH of 5.9 and measured at room temperature, corresponding to rather slow exchange rates as determined in Ref. 24. The high power of about  $5 \mu\text{T}$  applied with standard CEST protocols<sup>24</sup> to efficiently label fast-exchanging hydroxyl protons in glucose at physiological conditions is not achievable with bSSFP due to gradient hardware and SAR restrictions. The TR and flip angles used here for bSSFP imaging translate to a maximal power of only about  $0.5 \mu\text{T}$ . Figures 10a+b demonstrate that maximal AI values are reached in the slow-exchanging regime for  $\text{TR} = 2.5 \text{ ms} / \alpha_{\text{nom}} = 14^\circ$ . A similar behavior is observed at 3 T (Fig. 10a) and 9.4 T (Fig. 10b), however, with reduced effect strength at 9.4 T. In addition, the bSSFP asymmetry scales largely proportionally with the CEST pool size. In real glucose uptake experiments, the tissue glucose concentration is expected to be at least 10 times lower<sup>8</sup> in comparison to the 100 mM glucose solutions measured in this study, leading to AI values, which are hardly detectable for tissue-like relaxation times. Even in pathological tissues, e.g. in tumors where the glucose metabolism is increased and the relaxation times are prolonged, glucose-related bSSFP profile asymmetries can barely be detected (cf. Figs. 10a+b).

In the tissue homogenates where fibers are expected to be randomly distributed and microstructural anisotropy should be eliminated, a small but consistent residual bSSFP profile asymmetry was found which is likely to arise from CEST contributions. Due to the relatively low RF power of the bSSFP imaging protocol, this asymmetry is presumably caused by the NOE pool, which governs the chemical exchange processes at low power as verified based on the measurement of conventional CEST Z-spectra reconstructed at an RF power of  $0.5 \mu\text{T}$ , thus comparable to bSSFP. The standard deviations of the mean AI values in the assessed ROIs were relatively high considering the low bSSFPX asymmetry level. It is thus anticipated that it will be challenging to detect these effects in actual *in vivo* measurements.

Due to the larger chemical shift of the NOE pool as compared to the molecules studied in the initial bSSFPX work (choline, glucose, glycogen),<sup>7</sup> the bSSFP profile asymmetry in tissues is expected to depend highly on TR, in particular at higher field strengths (cf. Figs. 6c+d). Optimization of sequence parameters for NOE detection with bSSFPX in tissue would thus require exact *a priori* knowledge about the chemical shift difference of the contributing CEST pools, which is, however, hard to predict in practice. Similar to glucose, very short TRs ( $< 2 \text{ ms}$ ) are beneficial to provide detectable AI values (cf. Figs. 6c+d). If the chemical shift difference is larger than  $1/\text{TR}$  as it is the case for -3.5 ppm at both 3 T and 9.4 T, the CEST-related bSSFP asymmetry dip will fold back into the profile as a result of the periodicity of the bSSFP frequency response.<sup>7</sup> This behavior is evident in Figures 6c+d where it can be seen that the AI shows periodically occurring maxima as a function of TR. The amplitude of the maxima is, however, reduced the longer the TR.

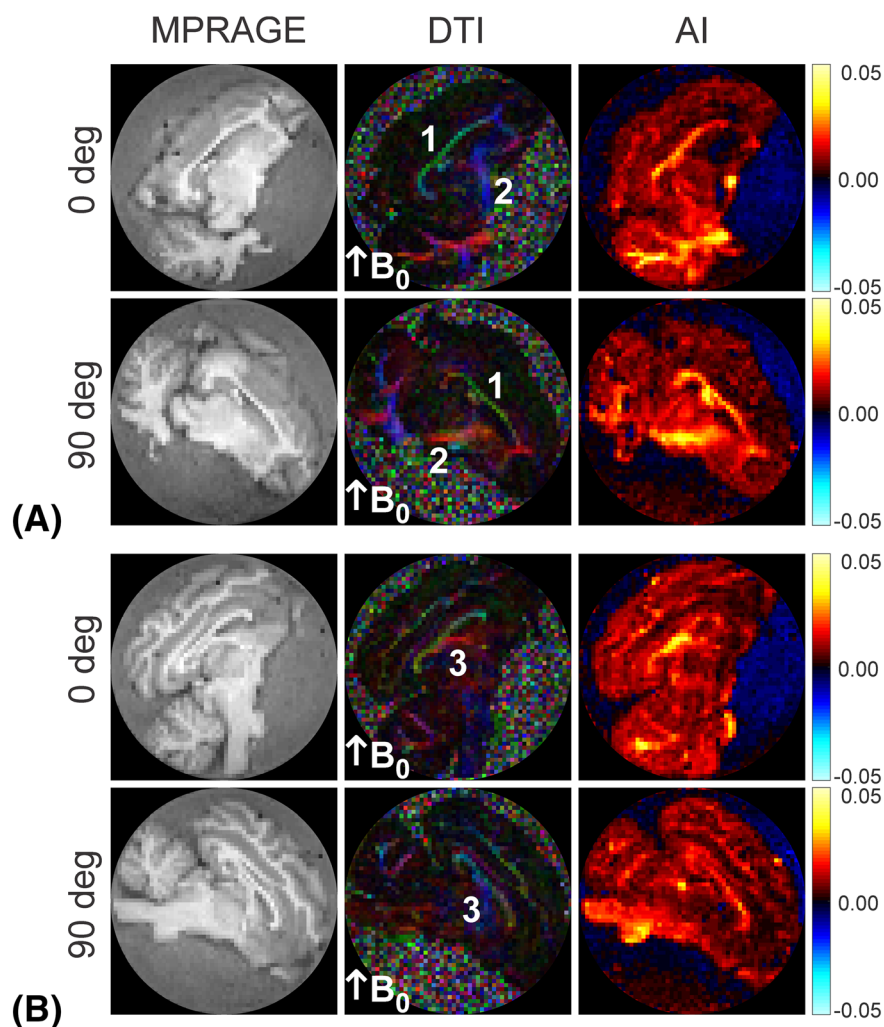


**FIGURE 7** Postmortem imaging of a fresh pig brain hemisphere at 3 T. The anatomical MPAGE contrast (left column), the color-coded principal diffusion direction map weighted by the fractional anisotropy (middle column; anterior-posterior  $\equiv$  green, superior-inferior  $\equiv$  blue, right-left  $\equiv$  red), and the asymmetry index (AI) map of bSSFPX (right column) are shown for two slices (A and B). To analyze the dependency of the bSSFP profile asymmetry on the orientation of the white matter fiber tracts with respect to  $B_0$  ( $\equiv$  superior-inferior axis, blue) the phantom was rotated by about  $90^\circ$  around the anterior-posterior axis as displayed in the second row of (A) and (B), respectively. The bSSFP frequency profile was assessed in the numbered ROIs; corpus callosum (1), corticospinal tract (2), and fornix (3)

Even though the MT pool is expected to be off-resonant with respect to bulk water,<sup>30</sup> it does not contribute to any asymmetry in the bSSFP profile since it is generally modeled with an ultrashort  $T_2$  relaxation time of only a few microseconds leading to a very broad frequency distribution. The simulations in Figures 10c+d demonstrate that the bSSFP profile asymmetry disappears if the NOE pool size is approaching zero even if an MT pool is still present. In fact, the presence of an MT pool slightly reduces the AI.

The bSSFP asymmetry in the tissue homogenates appears to depend only weakly on the tissue volume fractions (cf. Fig. 5). Dilution leads to two counteracting effects. First, the tissue concentration is reduced, which means that the CEST pool sizes are also reduced leading to lower AI values. Second, the relaxation times are prolonged resulting in higher AI values (cf. Figs. 10e+f). Due to these two counteracting effects, the AI values may not decrease substantially for lower tissue concentrations or may even increase.

The TR periodicity renders bSSFPX not only highly sensitive to the chemical shift difference of the target CEST pool but also to the static field strength  $B_0$  as evident from the simulations provided in Supporting Information Figure 1 for glucose (Fig. S1a) and NOE (Fig. S1b). It can be seen that the AI varies periodically as a function of the field strength for any given TR in the simulated range. Optimal sequence parameters to maximize the bSSFP profile asymmetry may thus vary depending on  $B_0$ . Optimization of the measurement protocol for maximal bSSFPX asymmetry is further complicated by gradient hardware and SAR limitations constraining the achievable minimal TR and maximal flip angle. Therefore, in contrast to standard CEST, the sensitivity of bSSFP to chemical exchange does not necessarily increase with higher fields as was observed in this study for the glucose measurements.

The results obtained in intact pig brain tissue reveal that the bSSFP profile asymmetry in white matter tracts with high fractional anisotropy is clearly driven by the fiber tract geometry and orientation relative to  $B_0$  (cf. Figs. 7 and 8) rather than chemical exchange processes as standard CEST imaging remains unaffected by the angle to  $B_0$  (cf. Fig. 9). The observed AI values in white matter tracts perpendicular to  $B_0$  are  $\approx 3$ -4 times higher than the AI levels measured in the homogenates, which is a major confounding factor in the direct detection of NOE effects with bSSFPX in white matter. On the other hand, this observation indicates that the observed asymmetries in white matter predominantly reflect the tissue microstructure and hardly any influence by chemical exchange.

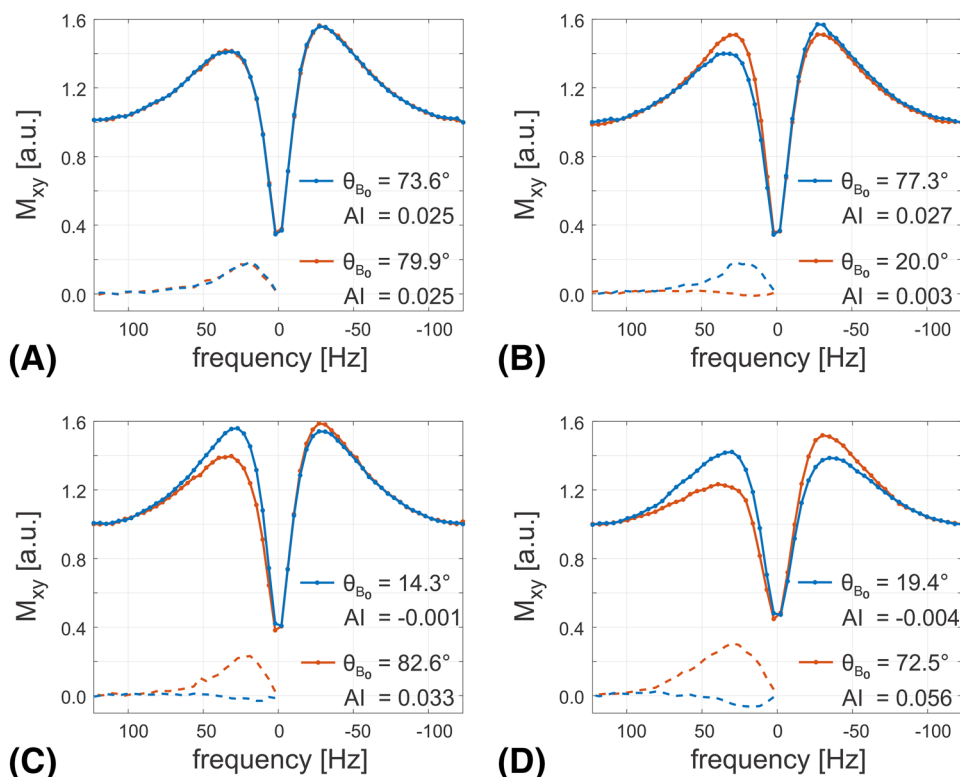


**FIGURE 8** The measured bSSFP frequency response (solid curves) and corresponding non-normalized asymmetries (dashed curves) in selected white matter structures of the pig brain along with the calculated normalized asymmetry indices (AI). At 3 T, ROIs are placed in the corpus callosum (A), fornix (B), and the corticospinal tract (C), as defined in Figure 7. An additional ROI assessed at 9.4 T in the corticospinal tract is shown in (D). Two different angles with respect to  $B_0$  ( $\theta_{B_0}$ ) are analyzed: initial position (blue curves) and  $\approx 90^\circ$  rotation about the anterior-posterior axis relative to the initial position (red curves). The bSSFP profiles are normalized by the passband signal level

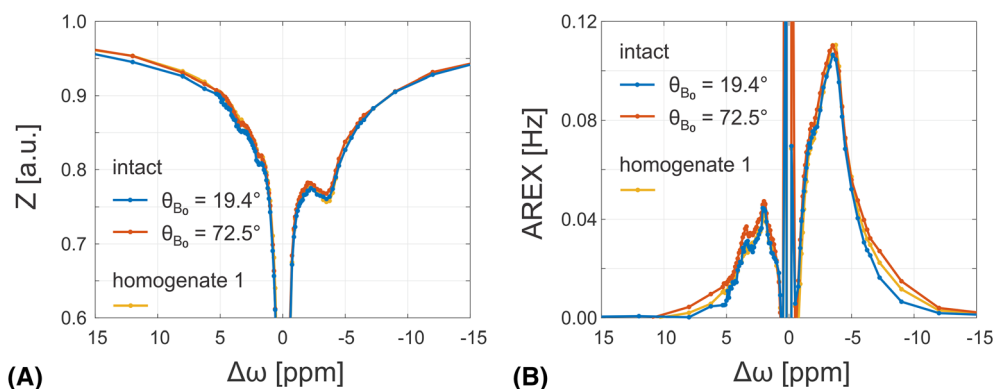


**FIGURE 9** A, Z-spectra reconstructed at an actual irradiation amplitude of  $B_{1,mean} = 0.5 \mu T$  from standard CEST experiments at 9.4 T. Mean Z-values are plotted for the marginally diluted tissue homogenate (homogenate 1, tissue volume fraction: 17/20, yellow curves) and an ROI in the corticospinal tract (identical to the one assessed for bSSFP in Fig. 8d) measured at two different angles relative to  $B_0$ : initial position (blue curves) and  $\approx 90^\circ$  rotated about the anterior-posterior axis relative to the initial position (red curves). B, Corresponding relaxation-compensated AREX spectra

The findings of this work emphasize that extrapolating results from single-solute phantoms with long relaxation times and no MT effects such as glucose water solutions can lead to overstating the sensitivity or specificity of a CEST technique. The measurement of tissue homogenates thus generally appears to be well suited for thorough *in vitro* validation of chemical exchange detection methods with regard to *in vivo* applications.

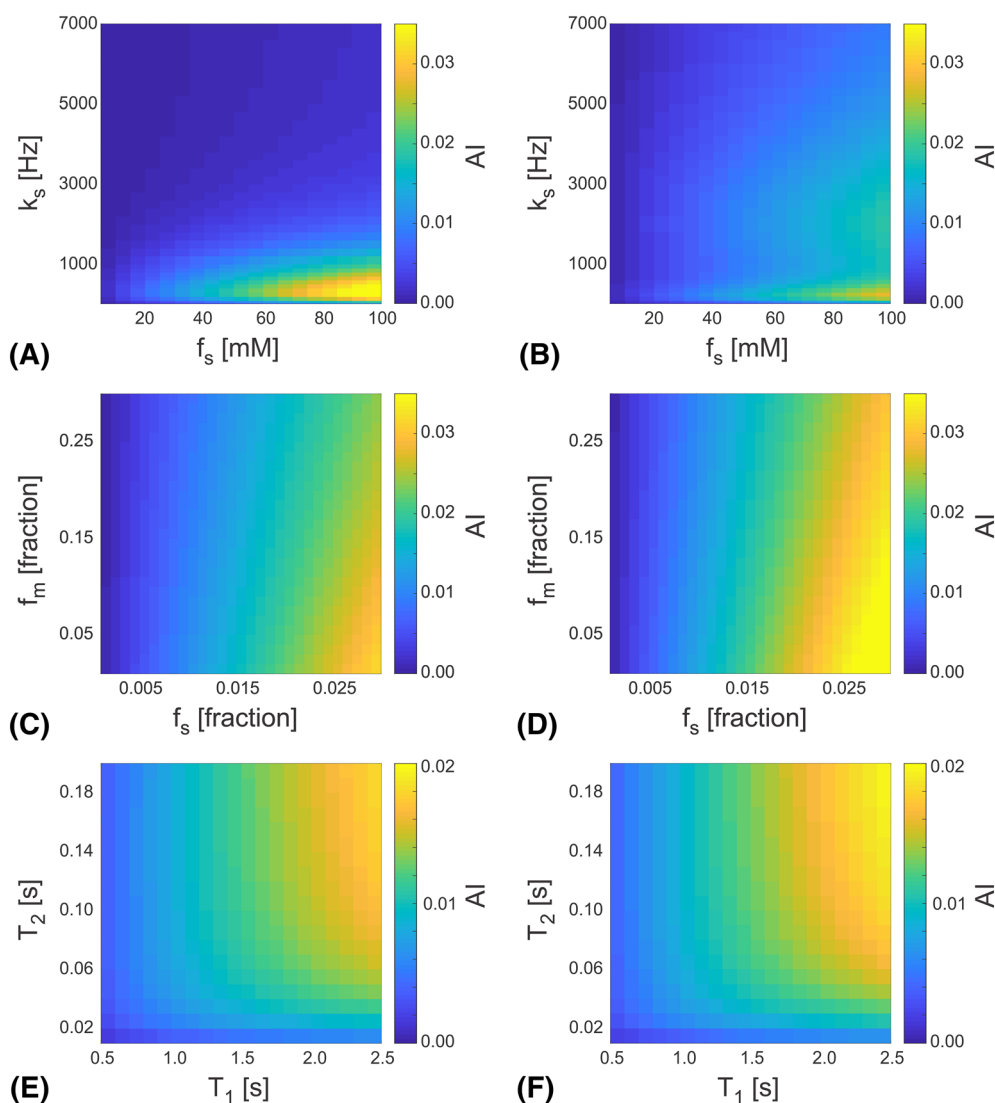


**FIGURE 10** A, B, The AI of the bSSFP frequency response calculated based on two-pool Bloch-McConnell simulations at 3 T (A) and 9.4 T (B) for glucose water solutions assuming hydroxyl protons resonating at  $\Delta_s = 1.28$  ppm relative to water. The AI is simulated as a function of the CEST pool concentration ( $f_s$  in units of mM) and the exchange rate ( $k_s$ ). C, D, E, F, The AI of the bSSFP frequency response calculated based on three-pool Bloch-McConnell simulations at 3 T (C, E) and 9.4 T (D, F) of a white matter tissue model (bulk water, NOE with a resonance at  $\Delta_s = -3.6$  ppm, MT centered at  $\Delta_m = -2.5$  ppm). The AI is simulated versus the NOE pool size fraction ( $f_s$ ) and the MT pool size fraction ( $f_m$ ) (C, D) as well as versus longitudinal and transverse relaxation times in the tissue range (E, F).

## 5 | CONCLUSION

The performed experiments have provided more insights into the underlying mechanisms driving asymmetries in the bSSFP frequency profile. It appears that chemical exchange processes are likely to contribute to a small but detectable degree to the bSSFP profile asymmetries observed in white matter.<sup>3</sup> However, due to the low asymmetry level in tissues, future work is needed to enable successful application of bSSFPX to *in vivo* targets. In particular, optimal sequence parameters such as TR, flip angle, or RF pulse shape have to be determined depending on the investigated field strength as well as the CEST pool of interest. In white matter structures with distinct fiber pathways, microstructural effects govern the bSSFP profile asymmetry and are barely affected by the low chemical exchange-related asymmetry levels. In such targets, reliable chemical exchange detection with bSSFPX will be hardly feasible.

## ACKNOWLEDGEMENT

We thank Hildegard Schulz for help with the preparation of the pig brain phantoms. The financial support of the Max Planck Society, the German Research Foundation (DFG, grant ZA 814/2-1, Reinhart Koselleck Project, DFG SCHE 658/12), and the European Union's Horizon 2020 research and innovation program (Grant Agreement No. 667510) is gratefully acknowledged. Open access funding enabled and organized by Projekt DEAL. [Correction added on 23 October 2020, after first online publication: Projekt Deal funding statement has been added.]



## FUNDING INFORMATION

Max Planck Society, German Research Foundation (DFG, grant ZA 814/2-1; Reinhart Koselleck Project, DFG SCHE 658/12), and European Union's Horizon 2020 research and innovation program (Grant Agreement No. 667510)

## ORCID

Rahel Heule  <https://orcid.org/0000-0002-4589-6483>

Anagha Deshmane  <https://orcid.org/0000-0003-0697-0895>

Moritz Zaiss  <https://orcid.org/0000-0001-9780-3616>

## REFERENCES

- Freeman R, Hill H. Phase and intensity anomalies in Fourier transform NMR. *J Magn Reson.* 1971;4:366-383.
- Miller KL. Asymmetries of the balanced SSFP profile. Part I: theory and observation. *Magn Reson Med.* 2010;63(2):385-395.
- Miller KL, Smith SM, Jezzard P. Asymmetries of the balanced SSFP profile. Part II: white matter. *Magn Reson Med.* 2010;63(2):396-406.
- Ehse P, Báez-Yáñez MG, Erb M, Scheffler K. Asymmetries of the balanced SSFP profile allow to probe microstructure anisotropy at 9.4 Tesla. Paper presented at: Proc. Intl. Soc. Mag. Reson. Med. Proceedings ISMRM 2017.
- Yablonskiy DA, Haacke EM. Theory of NMR signal behavior in magnetically inhomogeneous tissues: the static dephasing regime. *Magn Reson Med.* 1994;32(6):749-763.
- Xu T, Foxley S, Kleinjenshuis M, Chen WC, Miller KL. The effect of realistic geometries on the susceptibility-weighted MR signal in white matter. *Magn Reson Med.* 2018;79(1):489-500.
- Zhang S, Liu Z, Grant A, Keupp J, Lenkinski RE, Vinogradov E. Balanced Steady-State Free Precession (bSSFP) from an effective field perspective: Application to the detection of chemical exchange (bSSFPX). *J Magn Reson.* 2017;275:55-67.
- Walker-Samuel S, Ramasawmy R, Torrealdea F, et al. In vivo imaging of glucose uptake and metabolism in tumors. *Nat Med.* 2013;19(8):1067-1072.
- Zaiss M, Schuppert M, Deshmane A, et al. Chemical exchange saturation transfer MRI contrast in the human brain at 9.4T. *Neuroimage.* 2018;179:144-155.
- Deshmane A, Zaiss M, Lindig T, et al. 3D gradient echo snapshot CEST MRI with low power saturation for human studies at 3T. *Magn Reson Med.* 2019;81(4):2412-2423.
- Chung JJ, Choi W, Jin T, Lee JH, Kim SG. Chemical-exchange-sensitive MRI of amide, amine and NOE at 9.4 T versus 15.2 T. *NMR Biomed.* 2017;30(9):e3740. [https://authorservices.wiley.com/asset/photos/eLocators\\_text\\_for\\_author\\_site.pdf](https://authorservices.wiley.com/asset/photos/eLocators_text_for_author_site.pdf)
- Zaiss M, Ehse P, Scheffler K. Snapshot-CEST: Optimizing spiral-centric-reordered gradient echo acquisition for fast and robust 3D CEST MRI at 9.4 T. *NMR Biomed.* 2018;31(4):e3879. [https://authorservices.wiley.com/asset/photos/eLocators\\_text\\_for\\_author\\_site.pdf](https://authorservices.wiley.com/asset/photos/eLocators_text_for_author_site.pdf)
- Avdievich NI, Giapitzakis IA, Bause J, Shajan G, Scheffler K, Henning A. Double-row 18-loop transceive-32-loop receive tight-fit array provides for whole-brain coverage, high transmit performance, and SNR improvement near the brain center at 9.4T. *Magn Reson Med.* 2019;81(5):3392-3405.
- Fautz HP, Vogel M, Gross P, Kerr A, Zhu Y. B1 mapping of coil arrays for parallel transmission. Paper presented at: ISMRMProceedings ISMRM 2008.
- Chung S, Kim D, Breton E, Axel L. Rapid B1+ mapping using a preconditioning RF pulse with TurboFLASH readout. *Magn Reson Med.* 2010;64(2):439-446.
- Schuenke P, Windschuh J, Roeloffs V, Ladd ME, Bachert P, Zaiss M. Simultaneous mapping of water shift and B1 (WASABI)-Application to field-Inhomogeneity correction of CEST MRI data. *Magn Reson Med.* 2017;77(2):571-580.
- Zaiss M, Xu J, Goerke S, et al. Inverse Z-spectrum analysis for spillover-, MT-, and T1 -corrected steady-state pulsed CEST-MRI - application to pH-weighted MRI of acute stroke. *NMR Biomed.* 2014;27(3):240-252.
- Windschuh J, Zaiss M, Meissner JE, et al. Correction of B1-inhomogeneities for relaxation-compensated CEST imaging at 7 T. *NMR Biomed.* 2015;28(5):529-537.
- Mugler JP 3rd, Brookeman JR. Three-dimensional magnetization-prepared rapid gradient-echo imaging (3D MP RAGE). *Magn Reson Med.* 1990;15(1):152-157.
- Kellner E, Dhital B, Kiselev VG, Reiser M. Gibbs-ringing artifact removal based on local subvoxel-shifts. *Magn Reson Med.* 2016;76(5):1574-1581.
- Zaiss M, Bachert P. Exchange-dependent relaxation in the rotating frame for slow and intermediate exchange - modeling off-resonant spin-lock and chemical exchange saturation transfer. *NMR Biomed.* 2013;26(5):507-518.
- McConnell HM. Reaction Rates by Nuclear Magnetic Resonance. *J Chem Phys.* 1958;28(3):430-431.
- Zhou J, Wilson DA, Sun PZ, Klaus JA, Van Zijl PC. Quantitative description of proton exchange processes between water and endogenous and exogenous agents for WEX, CEST, and APT experiments. *Magn Reson Med.* 2004;51(5):945-952.
- Zaiss M, Anemone A, Goerke S, et al. Quantification of hydroxyl exchange of D-Glucose at physiological conditions for optimization of glucoCEST MRI at 3, 7 and 9.4 T. *NMR Biomed.* 2019;32(9):e4113.
- Henkelman RM, Huang X, Xiang QS, Stanisz GJ, Swanson SD, Bronskill MJ. Quantitative interpretation of magnetization transfer. *Magn Reson Med.* 1993;29(6):759-766.
- Zaiss M, Schmitt B, Bachert P. Quantitative separation of CEST effect from magnetization transfer and spillover effects by Lorentzian-line-fit analysis of z-spectra. *J Magn Reson.* 2011;211(2):149-155.

27. Liu D, Zhou J, Xue R, Zuo Z, An J, Wang DJ. Quantitative characterization of nuclear Overhauser enhancement and amide proton transfer effects in the human brain at 7 Tesla. *Magn Reson Med*. 2013;70(4):1070-1081.
28. van Zijl PCM, Lam WW, Xu J, Knutsson L, Stanisz GJ. Magnetization Transfer Contrast and Chemical Exchange Saturation Transfer MRI. Features and analysis of the field-dependent saturation spectrum. *Neuroimage*. 2018;168:222-241.
29. Stanisz GJ, Odobina EE, Pun J, et al. T1, T2 relaxation and magnetization transfer in tissue at 3T. *Magn Reson Med*. 2005;54(3):507-512.
30. Hua J, Jones CK, Blakeley J, Smith SA, van Zijl PC, Zhou J. Quantitative description of the asymmetry in magnetization transfer effects around the water resonance in the human brain. *Magn Reson Med*. 2007;58(4):786-793.

## SUPPORTING INFORMATION

Additional supporting information may be found online in the Supporting Information section at the end of the article.

**How to cite this article:** Heule R, Deshmane A, Zaiss M, Herz K, Ehses P, Scheffler K. Structure or Exchange? On the Feasibility of Chemical Exchange Detection with Balanced Steady-State Free Precession in Tissue – An In Vitro Study. *NMR in Biomedicine*. 2020; 33:e4200. <https://doi.org/10.1002/nbm.4200>